Second revised draft, submitted to the *IJSS* on 19 February 2020

A Unified Methodology for Computing the Stresses around an Arbitrarily-Shaped Hole in Isotropic or Anisotropic Materials

Ngurah Beni Setiawan[1] and Robert W. Zimmerman

Department of Earth Science and Engineering
Imperial College London, London, UK

Abstract

A unified semi-analytical solution based on graphical conformal mapping and complex variable methods is proposed to calculate the in-plane stress around an arbitrarily-shaped hole in isotropic or anisotropic materials. The method requires only the outline coordinates of the hole, the elastic moduli of the material, and the magnitude and direction of the far-field stresses. Comparison with many published results for a wide range of shapes, such as triangles, squares, ovaloids, and ellipses, has been carried out to validate the method. The method has also been applied to a highly irregular geometry that has been observed in a breakout of a subsurface borehole. The solution is essentially closed-form, in the sense that it can be explicitly expressed in terms of the mapping coefficients, and parameters that depend only on the elastic moduli of the materials. With such a degree of flexibility, the method will be useful to study the effect of hole geometry on the stress distribution around holes in isotropic or anisotropic materials.

Keywords: Conformal mapping; Complex variable; Lekhnitskii; anisotropic elasticity.

[1]Corresponding author: Ngurah Beni Setiawan, i.setiawan16@imperial.ac.uk, Department of Earth Science and Engineering, Imperial College London, London, SW7 2AZ, UK

1. Introduction

Accurate prediction of the stresses around underground openings or holes in mechanical components is of great importance, and is necessary for various purposes. Highway tunnels, underground mining, oil and gas wells, and other engineering designs often require preliminary evaluation to assess the stability and safety of the structure. In general, for such preliminary studies, the knowledge of the stress state acting around the structure, coupled with the strength characteristics of the material, is essential for predicting the potential risk. This can be addressed by means of analytical (or semi-analytical) solutions, or numerical analysis such as finite element or boundary element methods. Recent advances in computing capability have enabled such numerical analysis to become the standard procedure among practitioners and researchers. Nevertheless, analytical solutions are still very useful in providing upfront information about the stress state around openings in elastic materials. Moreover, analytical solutions offer a great advantage to allow for a parametric investigation for such preliminary analyses, such as the influence of material properties or the geometry of the openings.

Several authors have proposed analytical solutions for the calculation of elastic stresses around holes of various shapes. For instance, Daoust and Hoa[1] proposed a closed-form solution to investigate the stress around a triangular hole in anisotropic plates typically found in the design of aircraft windows. Gercek[2,3] investigated the stress around an arched roof with either a flat or parabolic floor, such as are widely used in mining and civil engineering. Greenspan[4] investigated square and ovaloid holes in isotropic plates, to assess the stress concentration around the hole contour. In general, the shape of the hole considered in their respective solutions involved simplified geometries such as a circle, ellipse, oval, triangle, square, or other shapes that slightly depart from such standard shapes; this is also true for the analytical solutions for various shapes of holes given by Lekhnitskii[5] and Savin[6].

In the above-mentioned studies, the stress is calculated using conformal mapping and the complex displacement potential method developed by Kolosov[7] and Muskhelisvili.[8] The conformal mapping facilitates the transformation of any given hole shape in one domain into a unit circle in another domain by an appropriate selection of the constants in the mapping function. The solution for the stress components will then be solved in this circular geometry using complex potentials. In practice, the challenge often lies in the determination of the mapping constants that can accurately reproduce the contour of interest, particularly in the regions associated with high stress concentration. It is therefore necessary to have an

appropriate mapping procedure that is capable of producing an approximated contour having a minimum misfit with the desired hole shape.

One such method is the Schwarz-Christoffel (SC) integral that applies for polygons. A comprehensive reference on this method has been written by Driscoll and Trefethen[9] and supplemented with a conformal mapping toolkit, *i.e.* a Matlab®-based program using the SC method. Despite its robustness, the SC method is mathematically complex, especially for holes having a relatively smooth contour with a continuously changing tangent. For this type of hole contour, it is possible to use a graphical approach proposed by Melentiev[10] that is mathematically more convenient.

Several authors[1-6,11-12] have solved specific problems in two-dimensional elasticity using a specific mapping function in which the conformal mapping coefficients of the hole are already known. Mitchell[13] and Exadaktylos *et al.*[14] presented a numerical approach to obtain appropriate conformal mapping constants for the stress calculation in a notched circular hole. Exadaktylos and Stavropoulou[15] proposed a method to compute the conformal mapping function for a hole described by numerical values of its boundary points, and applied it to the solution for the stresses around a horseshoe-shaped tunnel in an isotropic material. Sobey[16] implemented Melentiev's iterative procedure for a doubly-symmetric hole. Although the above-mentioned methods are general, in that they can be used for any shape of hole, these solutions pertain only to isotropic media.

Thus, it would be very useful to develop a method that allows the calculation of the stress around an arbitrary hole of given contour in isotropic or anisotropic media. This paper aims to propose a unified procedure in which the stress components around an arbitrary hole contour can be computed without *prior* knowledge of the conformal mapping constants. The hole contour, whose outline coordinate is known, is conformally mapped into a unit circle using the successive approximation method proposed by Melentiev. Although Melentiev's method is discussed in some detail in the monograph by Kantorovich and Krylov[17], there seem to be few if any examples of it being implemented, in the English-language open literature.

The proposed solution is derived by assuming that the material is anisotropic, and the body is subjected to a uniaxial far-field tensional or compressional stress. Using the principal of superposition, the solution can be extended to the more general case of biaxial loading. Moreover, by taking the two roots of the material characteristic equation to be nearly equal, *i.e.* $\mu_1 \approx \mu_2$ (see below), the solution can be used for isotropic materials. In this regard, see the discussion given by Gaede *et al.*[18]

Comparison with several published results for a wide range of possible shapes has been carried out to validate the method. As an example of a non-symmetrical and irregular shape, an actual wellbore shape reported by Zoback *et al.*[19] has been digitised, and the stress around the wellbore wall has been calculated to identify a region with high stress concentration.

In the subsequent sections, the procedure of conformal mapping using the graphical method proposed by Melentiev will be first discussed. Subsequently, the theory of complex stress and displacement potentials will be presented as the basis of the derivation of the proposed semi-analytical solution. Finally, a comparison with several published results will be presented.

2. Conformal mapping

Conformal mapping can be used to transform a region external to a given hole in the z-plane into the region external to the unit circle in the ξ–plane. (The mapping can also be done to the interior of the unit circle in the ξ-plane. In this paper, the mapping will be done from exterior to exterior). Kantorovich and Krylov[17] provide a detailed discussion of a graphical approach to conformal mapping that was originally developed by Melentiev[10]. Melentiev's method does not seem to have been used in the English-language open literature, although Sobey[16] used it in a report to the UK Ministry of Aviation in 1964. The procedure ensures that the region outside the unit circle is conformally mapped onto a simply connected region outside a hole in the z-plane, by an analytic function of the form

$$z = \sum_{k=0}^{\infty} m_k \xi^{1-k} = m_0 \xi + m_1 + m_2 \xi^{-1} + \cdots \tag{1}$$

in which $m_k = \alpha_k + i\beta_k$ are the complex conformal mapping coefficients, and $z = x + iy$. The function in eq. (1) maps the region outside of the unit circle in the ξ–plane into the region outside of the given contour in the z-plane.

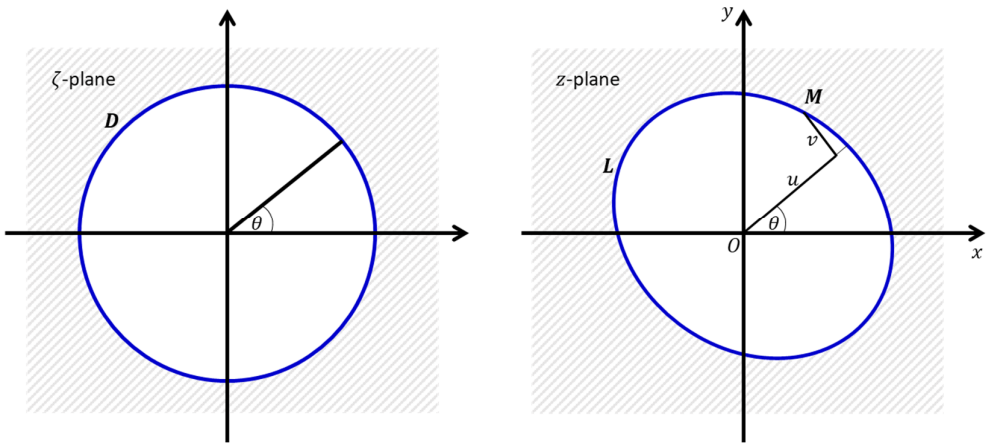

Figure 1. Conformal mapping of the region outside of unit circle in the in the ξ–plane into the region outside of a given contour in the z-plane.

In practice, the method of Melentiev involves mapping the unit circle in the ξ–plane onto the given contour in the z-plane. The required calculations therefore involve only points *on the two contours*, and hence many of the subsequent equations in this section are only intended to be valid on the unit circle, $|\xi| = 1$. However, the structure of eq. (1) guarantees that the mapping will be conformal throughout the regions outside of the two contours. On the circle $|\xi| = 1$, the Fourier series of the real and imaginary parts of z can be written as

$$x = \sum_{k=0}^{\infty} \alpha_k \cos(1-k)\theta - \beta_k \sin(1-k)\theta \tag{2}$$

$$y = \sum_{k=0}^{\infty} \beta_k \cos(1-k)\theta + \alpha_k \sin(1-k)\theta \tag{3}$$

Melentiev suggested working with the ratio $w = z/\xi$, rather than with z itself. This ratio can be written as

$$w = \frac{z}{\xi} = u + iv = \sum_{k=0}^{\infty} m_k \xi^{-k} \tag{4}$$

Hence, the expansion of u and v in a Fourier series can be written as[17]

$$u = \sum_{k=0}^{\infty} \alpha_k \cos k\theta + \beta_k \sin k\theta \tag{5}$$

$$v = \sum_{k=0}^{\infty} \beta_k \cos k\theta - \alpha_k \sin k\theta \tag{6}$$

Since both series contain the same coefficients, it is sufficient to only calculate one of the functions, u or v. Subsequent steps will therefore be based on eq. (5). Since in practice the mapping function must be truncated at a finite number of terms, a series containing $(M/2)+1$ terms will be constructed, *i.e.,*

$$z = \sum_{k=0}^{M/2} m_k \xi^{1-k} = m_0\xi + m_1 + m_2\xi^{-1} + \cdots + m_{M/2}\xi^{1-(M/2)} \tag{7}$$

which leads to

$$w = \frac{z}{\xi} = \sum_{k=0}^{M/2} m_k \xi^{-k} = m_0 + m_1\xi^{-1} + m_2\xi^{-2} + \cdots + m_{M/2}\xi^{-(M/2)} \tag{8}$$

so that *on the contour*, the real part of *w* takes the form

$$u = \sum_{k=0}^{M/2} \alpha_k \cos k\theta + \beta_k \sin k\theta \tag{9}$$

The total angle 2π of the circle in the ξ-plane is now divided into M equal parts. Sets of rays are constructed from the origin (Fig. 2). By allowing the angle θ to take on the values $2\pi/M$, $4\pi/M$, ... ,2π, the value of u for each ray can be calculated as follows:

$$u_1 = \sum_{k=0}^{M/2} \alpha_k \cos\left(\frac{2\pi k}{M}\right) + \beta_k \sin\left(\frac{2\pi k}{M}\right) \tag{10}$$

$$\cdots u_M = \sum_{k=0}^{M/2} \alpha_k \cos(2\pi k) + \beta_k \sin(2\pi k) \tag{11}$$

This set of equations can be solved for the coefficients α_k and β_k, as follows[17]:

$$\alpha_k = \frac{2}{M}\sum_{n=1}^{M} u_n \cos\left(\frac{2\pi nk}{M}\right) \tag{12}$$

$$\alpha_0 = \frac{1}{M}\sum_{n=1}^{M} u_n \tag{13}$$

$$\alpha_{M/2} = \frac{1}{M}\sum_{n=1}^{M} (-1)^n u_n \tag{14}$$

$$\beta_k = \frac{2}{M}\sum_{n=1}^{M} u_n \sin\left(\frac{2\pi nk}{M}\right) \tag{15}$$

$$\beta_0 = -\sum_{n=1}^{M/2} \beta_n \tag{16}$$

Although the final coefficient $\beta_{M/2}$ cannot be computed, for a sufficiently large value of M, this coefficient can be taken to be zero.[17]

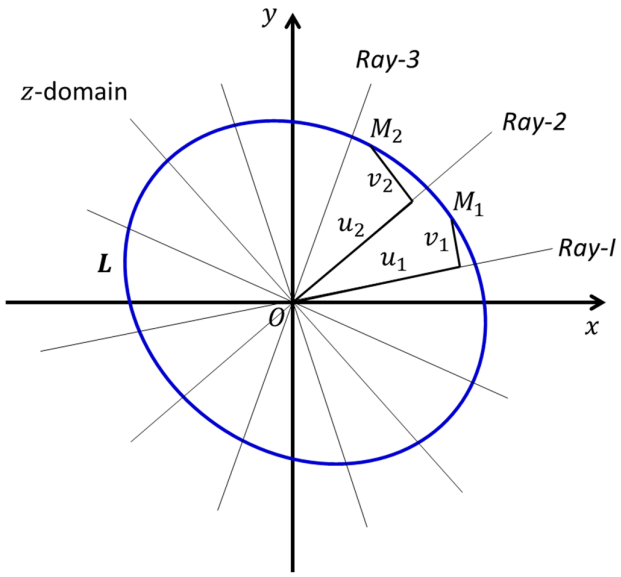

Figure 2. Construction of rays around the shape in the z-plane.

An iterative process is required to determine the most appropriate values of the coefficients α_k such β_k such that the approximated contour is as close as possible to the desired contour in the z-plane. For instance, assume that some values for $\{u_1, u_2, \dots, u_M\}$ have successfully been determined. The coefficients α_k such β_k can then be calculated from the equations given above. The v_n can then be calculated as

$$v_n = \sum_{k=0}^{M/2} \beta_k \cos\left(\frac{2\pi nk}{M}\right) - \alpha_k \sin\left(\frac{2\pi nk}{M}\right) \tag{17}$$

Finally, by using u_n and v_n, the points $\{M'_1, M'_2, \dots, M'_M\}$ can be constructed as an approximation to the desired values of $\{M_1, M_2, \dots, M_M\}$ that lie on curve L in the z-plane (Fig. 1). However, it will generally not be the case that the initial values of u_n, which can be denoted by $\left\{u_1^{(0)}, u_2^{(0)}, \dots, u_M^{(0)}\right\}$, satisfy the desired condition in the first instance, *i.e.* the initial estimated values $\left\{M_1^{(0)}, M_2^{(0)}, \dots, M_M^{(0)}\right\}$ will slightly depart from the desired values $\{M_1, M_2, \dots, M_M\}$.

Melentiev[10] proposed an iterative method to transfer the value M'_n to be arbitrarily close to the desired position M_n. As illustrated in Fig. 3, a line is drawn from the point $M_n^{(0)}$ to

the origin, and the intersection of this line with the curve L is taken to be the new point $M_n^{(1)}$. The ray $O{-}M_n^{(1)}$ is then projected onto the ray $O{-}u_n^{(0)}$, which defines the new value, $u_n^{(1)}$.

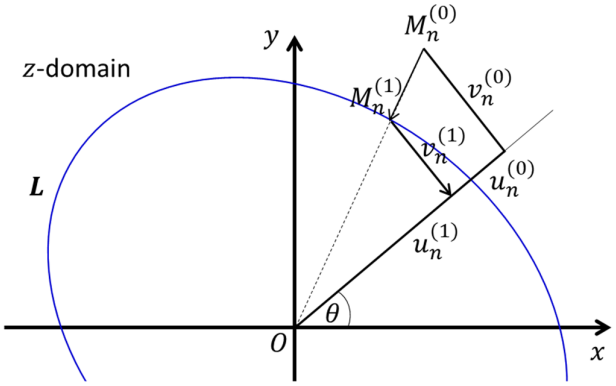

Figure 3. A step in the iterative procedure to transfer point $M_n^{(0)}$ to the contour L.

To start the computation, the first approximation, $u_n^{(0)}$, is taken as

$$u_n^{(0)} = \frac{1}{M}\sum_{k=1}^{M}(x_k + y_k) \tag{18}$$

The $v_n^{(0)}$ values can then be computed from eq. (17), thereby locating the initial point, $M_n^{(0)}$. The misfit between $M_n^{(0)}$ and the desired value M_n can be quantified as follows:

$$\varepsilon = \frac{1}{M}\sqrt{\sum_{n=1}^{M}\left(u_n^{(i+1)} - u_n^{(i)}\right)^2} \tag{19}$$

Iterations continue until ε is less than some tolerance, taken here to be 10^{-6}.

Figure 4 shows an example of the region outside a triangle conformally mapped into the region outside the unit circle. The closed curves and quasi-radial lines in the z-plane correspond to constant values of the angular and radial coordinates in the ξ-plane. The orthogonality of these curves in the z-plane shows that the mapping is indeed conformal.

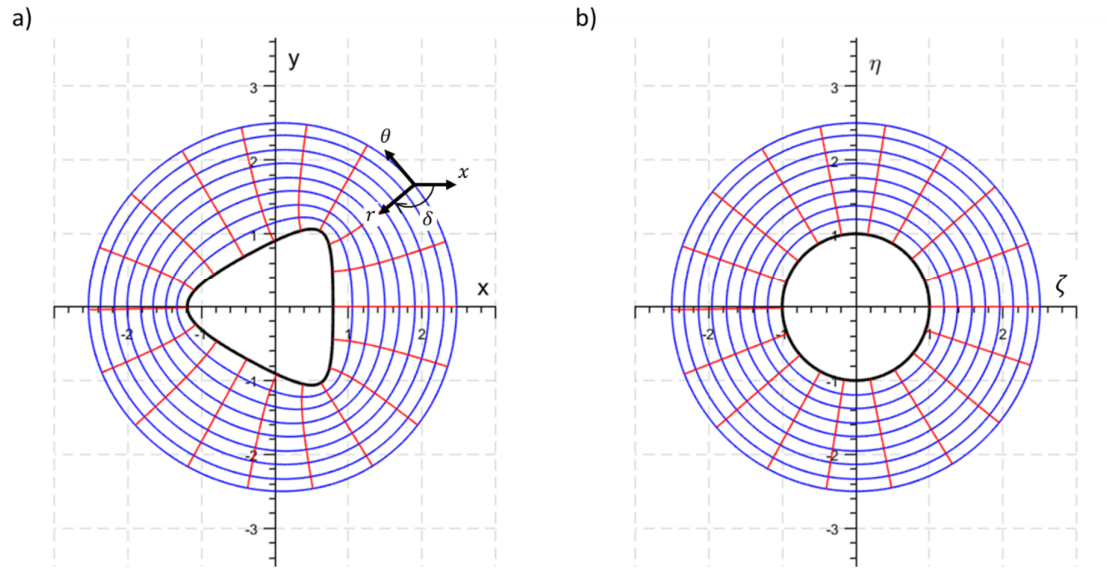

Figure 4. Conformal mapping of the region outside a triangular shape in the z-plane into the region outside the unit circle in the ξ-plane.

3. Complex stress-displacement potentials in anisotropic elastic materials

For a plane problem in elasticity, under the plane stress assumptions of $\sigma_{zz} = \sigma_{yz} = \sigma_{xz} = 0$, the generalised Hooke's law can be written as

$$\begin{bmatrix} \varepsilon_{xx} \\ \varepsilon_{yy} \\ \gamma_{xy} \end{bmatrix} = \begin{bmatrix} a_{11} & a_{12} & a_{16} \\ a_{12} & a_{22} & a_{26} \\ a_{16} & a_{26} & a_{66} \end{bmatrix} \begin{bmatrix} \sigma_{xx} \\ \sigma_{yy} \\ \sigma_{xy} \end{bmatrix} \tag{20}$$

where the $\{a_{ij}\}$ are the elastic compliances of the material. The stress components can be written in terms of the Airy stress function $U(x, y)$, as follows:

$$\sigma_{xx} = \frac{\partial^2 U}{\partial y^2} \qquad \sigma_{yy} = \frac{\partial^2 U}{\partial x^2} \qquad \sigma_{xy} = -\frac{\partial^2 U}{\partial x \partial y} \tag{21}$$

For a plane problem, the only non-trivial compatibility relation is

$$\frac{\partial^2 \varepsilon_{xx}}{\partial y^2} + \frac{\partial^2 \varepsilon_{yy}}{\partial x^2} - \frac{\partial^2 \gamma_{xy}}{\partial x \partial y} = 0 \tag{22}$$

If the constitutive equation (20) is inserted into the compatibility relation, (22), the following governing fourth-order partial differential equation is obtained:

$$a_{22}\frac{\partial^4 U}{\partial x^4} - 2a_{26}\frac{\partial^4 U}{\partial x^3 \partial y} + (2a_{12} + a_{66})\frac{\partial^4 U}{\partial x^2 \partial y^2} - 2a_{16}\frac{\partial^4 U}{\partial x \partial y^3} + a_{11}\frac{\partial^4 U}{\partial y^4} = 0 \tag{23}$$

The solution to this PDE depends on following characteristic equation,

$$a_{11}\mu^4 - 2a_{16}\mu^3 + (2a_{12} + a_{66})\mu^2 - 2a_{26}\mu + a_{22} = 0 \tag{24}$$

the four roots of which can be written as

$$\mu_1 = \gamma_1 + i\delta_1, \quad \bar{\mu}_1 = \gamma_1 - i\delta_1, \quad \mu_2 = \gamma_2 + i\delta_2, \quad \bar{\mu}_2 = \gamma_2 - i\delta_2 \tag{25}$$

The general solution for the Airy stress function can be written in terms of two complex potentials, $F_1(z_1)$ and $F_2(z_2)$, as[21]

$$U(x,y) = F_1(z_1) + F_2(z_2) + \overline{F_1(z_1)} + \overline{F_2(z_2)} \tag{26}$$

where $z_j = x + \mu_j y$. Two new complex functions that are the derivatives of the original pair are now defined as

$$\phi(z_1) = F_1'(z_1), \quad \psi(z_2) = F_2'(z_2) \tag{27}$$

Finally, the in-plane stress components can be expressed as follows:

$$\sigma_{xx} = 2Re[\mu_1^2\phi'(z_1) + \mu_2^2\psi'(z_2)] \tag{28}$$

$$\sigma_{yy} = 2Re[\phi'(z_1) + \psi'(z_2)] \tag{29}$$

$$\sigma_{xy} = -2Re[\mu_1\phi'(z_1) + \mu_2\psi'(z_2)] \tag{30}$$

The roots of the characteristic equation (24) depend on the material's elastic moduli. Three cases are possible. The roots may be complex and different, they may be complex and equal, or they may be different and purely imaginary. Some specific examples are given by Lekhnitskii[5], who points out that the case of purely real roots can be ruled out by energy considerations. Finally, note that to apply this formalism to the problem of plane strain, it is merely necessary to replace $\{a_{ij}\}$ in the characteristic equation with $c_{ij} = a_{ij} - a_{i3}a_{3j}/a_{33}$.

4. Solution for the stresses around an arbitrarily-shaped hole

To find the stresses around an arbitrarily-shaped hole in a medium subject to a given far-field stress, the two stress potentials defined in eq. (27) need to be found. Recall the mapping function given by eq. (1), truncated to *N* terms:

$$z = \omega(\xi) = \sum_{k=0}^{N} m_k \xi^{1-k} \tag{31}$$

The auxiliary variables $\boldsymbol{z_1}$ and $\boldsymbol{z_2}$ are related to $\boldsymbol{z}$ by[6,12,20]

$$z_1 = x + \mu_1 y = \frac{(1 - i\mu_1)}{2} z + \frac{(1 + i\mu_1)}{2} \bar{z} \tag{32}$$

and similarly for z_2. Substituting eq. (31) into eq. (32) yields, for j = 1 or 2,

$$z_j = \frac{1}{2}\sum_{k=0}^{N} (1 - i\mu_j)\alpha_k \xi^{1-k} + (1 + i\mu_j)\alpha_k \bar{\xi}^{1-k} + (i + \mu_j)\beta_k \xi^{1-k} + (\mu_j - i)\beta_k \bar{\xi}^{1-k} \tag{33}$$

On the unit circle, where $\xi = e^{i\theta}$ and $\bar{\xi} = e^{-i\theta} = 1/\xi$, these relations take the form

$$z_j = \frac{1}{2}\sum_{k=0}^{N}(1 - i\mu_j)\alpha_k \xi^{1-k} + (1 + i\mu_j)\alpha_k \xi^{-(1-k)} + (i + \mu_j)\beta_k \xi^{1-k} + (\mu_j - i)\beta_k \xi^{-(1-k)} \tag{34}$$

The complex potentials defined above must also satisfy the following boundary conditions on the hole contour[5,21]

$$2Re[\phi(z_1) + \psi(z_2)] = -\int_0^S Y_n\, ds + C_1 \equiv f_1 \tag{35}$$

$$2Re[\mu_1\phi(z_1) + \mu_2\psi(z_2)] = \int_0^S X_n\, ds + C_2 \equiv f_2 \tag{36}$$

where X_n and Y_n are the traction components acting on the hole contour, S is a point on the contour, and the C_i are constants of integration. The focus of the present paper is on the problem of a traction-free hole in an infinite body, subjected to a far-field state of uniform stress. In this case, $X_n = Y_n = 0$. Moreover, although the C_i will influence the displacements, they have no effect on the stresses, and so for the present purposes they can be set to 0. Consequently, $f_1 = f_2 = 0$ in the two previous equations.

In this case, the two potentials take the following general form[6]

$$\phi(z_1) = B^* z_1 + \phi_0(z_1), \qquad \psi(z_2) = (B'^* + iC'^*)z_2 + \psi_0(z_2) \tag{37}$$

where the potentials having subscript 0 are analytical functions outside of the hole, and the constants can be expressed in terms of the far-field stresses, as follows:

$$B^* = \frac{\sigma_{xx}^{\infty} + (\gamma_2^2 + \delta_2^2)\sigma_{yy}^{\infty} + 2\gamma_2\sigma_{xy}^{\infty}}{2[(\gamma_2 - \gamma_1)^2 + (\delta_2^2 - \delta_1^2)]} \tag{38}$$

$$B'^* = \frac{(\gamma_1^2 - \delta_1^2 - 2\gamma_1\gamma_2)\sigma_{yy}^{\infty} - \sigma_{xx}^{\infty} - 2\gamma_2\sigma_{xy}^{\infty}}{2[(\gamma_2 - \gamma_1)^2 + (\delta_2^2 - \delta_1^2)]} \tag{39}$$

$$C'^* = \frac{(\gamma_2 - \gamma_1)\sigma_{xx}^{\infty} + [\gamma_2(\gamma_1^2 + \delta_1^2) - \gamma_1(\gamma_2^2 + \delta_2^2)]\sigma_{yy}^{\infty} + [(\gamma_1^2 + \delta_1^2) - (\gamma_2^2 + \delta_2^2)]\sigma_{xy}^{\infty}}{2\delta_2[(\gamma_2 - \gamma_1)^2 + (\delta_2^2 - \delta_1^2)]} \tag{40}$$

Substitution of eq. (37) into eqs. (35) and (36) shows that the 0-subscripted potentials must satisfy the following boundary conditions:

$$2Re[\phi_0(z_1) + \psi_0(z_2)] = -2Re[B^* z_1 + (B'^* + iC'^*)z_2] \equiv f_1^0 \tag{41}$$

$$2Re[\mu_1\phi_0(z_1) + \mu_2\psi_0(z_2)] = -2Re[\mu_1 B^* z_1 + \mu_2(B'^* + iC'^*)z_2] \equiv f_2^0 \tag{42}$$

By combining eqs. (41) and (34), the first boundary function can be expressed, on the hole contour, as[20]

$$f_1^0 = -\frac{1}{2}\left[\begin{array}{l}(K_1+\overline{K}_2)\sum_{k=0}^{N}\alpha_k\,\xi^{1-k} + (\overline{K}_1+K_2)\sum_{k=0}^{N}\alpha_k\,\xi^{-(1-k)} \\ +(K_3+\overline{K}_4)\sum_{k=0}^{N}\beta_k\xi^{1-k} + (\overline{K}_3+K_4)\sum_{k=0}^{N}\beta_k\,\xi^{-(1-k)}\end{array}\right] \tag{43}$$

in which the constants K_i are defined by

$$\begin{aligned} &K_1 = B^*(1-i\mu_1) + (B'^* + iC'^*)(1-i\mu_2), \quad K_2 = B^*(1+i\mu_1) + (B'^* + iC'^*)(1+i\mu_2) \\ &K_3 = B^*(\mu_1+i) + (B'^* + iC'^*)(\mu_2+i), \qquad K_4 = B^*(\mu_1-i) + (B'^* + iC'^*)(\mu_2-i) \end{aligned} \tag{44}$$

Following the same process, the second boundary function can be expressed, on the hole contour, as

$$f_2^0 = -\frac{1}{2}\left[\begin{array}{l}(K_5+\overline{K}_6)\sum_{k=0}^{N}\alpha_k\,\xi^{1-k} + (\overline{K}_5+K_6)\sum_{k=0}^{N}\alpha_k\,\xi^{-(1-k)} \\ +(K_7+\overline{K}_8)\sum_{k=0}^{N}\beta_k\xi^{1-k} + (\overline{K}_7+K_8)\sum_{k=0}^{N}\beta_k\,\xi^{-(1-k)}\end{array}\right] \tag{45}$$

in which the constants K_i are defined by

$$\begin{aligned} &K_5 = \mu_1 B^*(1-i\mu_1) + \mu_2(B'^* + iC'^*)(1-i\mu_2), \quad K_6 = \mu_1 B^*(1+i\mu_1) + \mu_2(B'^* + iC'^*)(1+i\mu_2) \\ &K_7 = \mu_1 B^*(\mu_1+i) + \mu_2(B'^* + iC'^*)(\mu_2+i), \qquad K_8 = \mu_1 B^*(\mu_1-i) + \mu_2(B'^* + iC'^*)(\mu_2-i) \end{aligned} \tag{46}$$

It can be verified that, on the unit circle, both expressions (43) and (45) are purely real, as required by eqs. (41) and (42).

Since $z_1$and z_2 are each known functions of ξ, the two 0-subscripted potentials, which can now be denoted as $\phi_0(\xi)$ and $\psi_0(\xi)$, can be found by contour integration, as explained on p. 155 of Savin[6], modified to account for the fact that in the current formulation, the mapping is made from the region *outside* the unit circle, rather than inside the unit circle:

$$\phi_0(\xi) = \frac{-i}{4\pi(\mu_1-\mu_2)}\int_\gamma (\mu_2 f_1^0 - f_2^0)\frac{t+\xi}{t-\xi}\frac{dt}{t} + \lambda_1 \tag{47}$$

$$\psi_0(\xi) = \frac{i}{4\pi(\mu_1-\mu_2)}\int_\gamma (\mu_1 f_1^0 - f_2^0)\frac{t+\xi}{t-\xi}\frac{dt}{t} + \lambda_1 \tag{48}$$

where γ is the unit circle in the ξ-plane, and the λ_i are constants whose values are known, but which will be ignored here, as they have no influence on the stresses. Note that this formula is usually discussed for situations in which the *interior* of the unit circle in the ξ-plane is mapped into the region outside of the physical hole. In the present formulation, the exterior of the unit circle in the ξ-plane has been mapped into the region outside of the physical hole. The connection between the two situations is discussed by Muskhelishvili[8], p. 268. The two

approaches are essentially identical, since one can imagine a two-stage mapping in which the first stage is an inversion, $\xi = 1/s$, that first maps the interior of the unit circle into its exterior. This would merely change the signs of the power exponents in the mapping function given by eq. (1), but would not change the numerical values of the mapping coefficients.

In light of eqs. (43) and (45), the parenthesised terms in eqs. (47) and (48) are series that involve terms of the form t^n, for non-zero integer values of n. Since the relevant values of ξ lie outside the unit circle, the integrals have the following values[22]:

$$\int_\gamma t^n \cdot \frac{t+\xi}{t-\xi}\frac{\mathrm{d}t}{t} = 0, \qquad \int_\gamma \frac{1}{t^n} \cdot \frac{t+\xi}{t-\xi}\frac{\mathrm{d}t}{t} = -4\pi i \xi^{-n} \tag{49}$$

in which n is taken to be a positive integer, and a constant term on the right side of each integral has been ignored, as they do not contribute to the stresses. Note also that the m_1 term in the mapping function (1), which would contribute terms in the integrand having $k-1=n=0$, represents a rigid-body translation of the hole contour, and therefore has no influence on the boundary stresses. Non-zero values of m_1 that may be generated by the Melentiev iterative mapping procedure can therefore be set to zero, when computing the stresses. Hence, there is no need to consider the case $n = 0$ in eq. (49).

Substituting f_1^0 and f_2^0 from eqs. (42) and (45) into expressions (47) and (48), and making use of the integrals in eq. (49), leads to the following expressions for the two potentials:

$$\phi_0(\xi) = A_1\alpha_0\xi^{-1} + A_2\beta_0\xi^{-1} + A_3\sum_{k=2}^{N}\alpha_k\,\xi^{1-k} + A_4\sum_{k=2}^{N}\beta_k\,\xi^{1-k} \tag{50}$$

$$\psi_0(\xi) = A_5\alpha_0\xi^{-1} + A_6\beta_0\xi^{-1} + A_7\sum_{k=2}^{N}\alpha_k\,\xi^{1-k} + A_8\sum_{k=2}^{N}\beta_k\,\xi^{1-k} \tag{51}$$

in which the constants A_i are given by

$$A_1 = \frac{1}{2(\mu_1-\mu_2)}[\mu_2(\overline{K}_1+K_2) - (\overline{K}_5+K_6)] \tag{52}$$

$$A_2 = \frac{1}{2(\mu_1-\mu_2)}[\mu_2(\overline{K}_3+K_4) - (\overline{K}_7+K_8)] \tag{53}$$

$$A_3 = \frac{1}{2(\mu_1-\mu_2)}[\mu_2(K_1+\overline{K}_2) - (K_5+\overline{K}_6)] \tag{54}$$

$$A_4 = \frac{1}{2(\mu_1-\mu_2)}[\mu_2(K_3+\overline{K}_4) - (K_7+\overline{K}_8)] \tag{55}$$

$$A_5 = \frac{-1}{2(\mu_1-\mu_2)}[\mu_1(\overline{K}_1+K_2) - (\overline{K}_5+K_6)] \tag{56}$$

$$A_6 = \frac{-1}{2(\mu_1 - \mu_2)}[\mu_1(\overline{K}_3 + K_4) - (\overline{K}_7 + K_8)] \tag{57}$$

$$A_7 = \frac{-1}{2(\mu_1 - \mu_2)}[\mu_1(K_1 + \overline{K}_2) - (K_5 + \overline{K}_6)] \tag{58}$$

$$A_8 = \frac{-1}{2(\mu_1 - \mu_2)}[\mu_1(K_3 + \overline{K}_4) - (K_7 + \overline{K}_8)] \tag{59}$$

The stress components can now be calculated as

$$\sigma_{xx} = \sigma_{xx}^{\infty} + 2Re\left[\mu_1^2 \phi'_0(z_1) + \mu_2^2 \psi'_0(z_2)\right] \tag{60}$$

$$\sigma_{yy} = \sigma_{yy}^{\infty} + 2Re\left[\phi'_0(z_1) + \psi'_0(z_2)\right] \tag{61}$$

$$\sigma_{xy} = \sigma_{xy}^{\infty} - 2Re[\mu_1 \phi'_0(z_1) + \mu_2 \psi'_0(z_2)] \tag{62}$$

in which the derivatives of the potentials can be computed using the chain rule, as follows:

$$\phi'_0(z_1) = \frac{d\phi_0(\xi)}{d\xi}\frac{d\xi}{dz_1} = \frac{\phi'_0(\xi)}{\omega'_1(\xi)} \tag{63}$$

$$\psi'_0(z_2) = \frac{d\psi_0(\xi)}{d\xi}\frac{d\xi}{dz_2} = \frac{\psi'_0(\xi)}{\omega'_2(\xi)} \tag{64}$$

The tangential and radial stress components can be calculated using the following transformation[23]:

$$\sigma_{\theta\theta} - \sigma_{rr} + 2\sigma_{r\theta} = \left(\sigma_{xx} - \sigma_{yy} + 2\sigma_{xy}\right)e^{2i\delta} \tag{65}$$

$$\sigma_{\theta\theta} + \sigma_{rr} = \sigma_{xx} + \sigma_{yy} \tag{66}$$

in which δ is the rotational angle from the x-axis to the radial axis r (see Fig. 4). For biaxial tension or compression, the principal of superposition can be used.

5. Validation of the proposed methodology

The general workflow of the proposed method is as follows. The hole contour, whose outline coordinates are known in the z-plane, is conformally mapped into the outside of the unit circle using Melentiev's successive approximation method, to obtain the mapping coefficients, m_k. The characteristic equation (24) is then solved for the characteristic roots, after which the *B* and *C* constants appearing in the stress potentials can be computed from knowledge of these roots and the far-field stresses, using eqs. (38-40). The potentials are then given by eqs. (50,51), and the derivatives of the two potentials are calculated using eqs. (63,64). The stress components can then be calculated using eqs. (60-62), and can be converted into polar coordinates using eqs. (65,66).

To demonstrate the robustness of this method, the following section provides validation

by comparing the stresses obtained with the proposed method against several known formulations and published results. The validation covers a wide range of possible shapes, such as ellipses, triangles, squares, ovaloids, *etc.*, in both isotropic and anisotropic plates.

5.1 Elliptical hole

For an elliptical hole in isotropic medium, Jaeger *et al.*[23] showed that the stress concentration around the hole contour is given by the following equation:

$$\sigma_\theta = \sigma^\infty \left[\frac{2ab + (a^2 - b^2)\cos 2\alpha - (a+b)^2 \cos 2(\alpha - \chi)}{(a^2 + b^2) - (a^2 - b^2)\cos 2\chi} \right] \tag{67}$$

in which α denotes the angle between the direction of the far-field stress σ^∞ with the x-axis, and a and b are the lengths of the ellipse's axes in the x and y directions, respectively. Figure 5 shows ellipses with $a/b = 3/2$ and $a/b = 2/3$. The elliptical coordinate χ is related to the polar coordinate θ by $\tan\chi/\tan\theta = a/b$ [22]. Savin[6] gave the following alternative expression for the hoop stress in this problem:

$$\sigma_\theta = \sigma^\infty \left[\frac{(1+k)^2 \sin^2(\theta + \alpha) - \sin^2\alpha - k^2 \cos^2\alpha}{\sin^2\theta + k^2 \cos^2\theta} \right] \tag{68}$$

in which $k = b/a$.

The conformal mapping constants for an ellipse with $a/b = 3/2$ that are obtained using Melentiev's method, with seven terms in the mapping function, are $m_0 = 0.9976$, $m_1 = 0.0017$, $m_2 = 1.999$, $m_3 = 0.0002$ and $m_4 = m_5 = m_6 = 0.0001$. The hoop stresses that are computed with the present method are compared in Fig. 6 to those given by the analytical expressions (67) and (68), for three different orientations of the far-field stress. The agreement is extremely good, for all angles around the ellipse, and for all three loading cases.

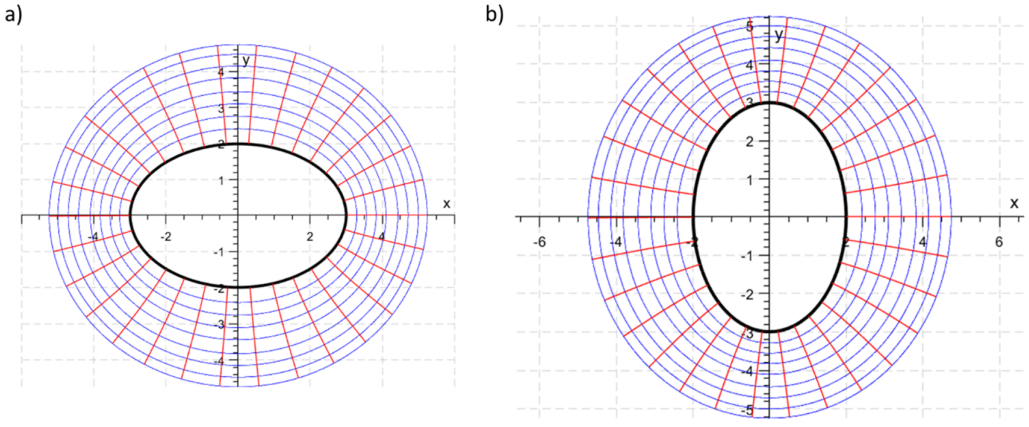

Figure 5. Elliptical holes with (a) $a/b = 3/2$ and (b) $a/b = 2/3$, showing the mapped curves that correspond to the lines of constant r and constant θ in the ξ-plane.

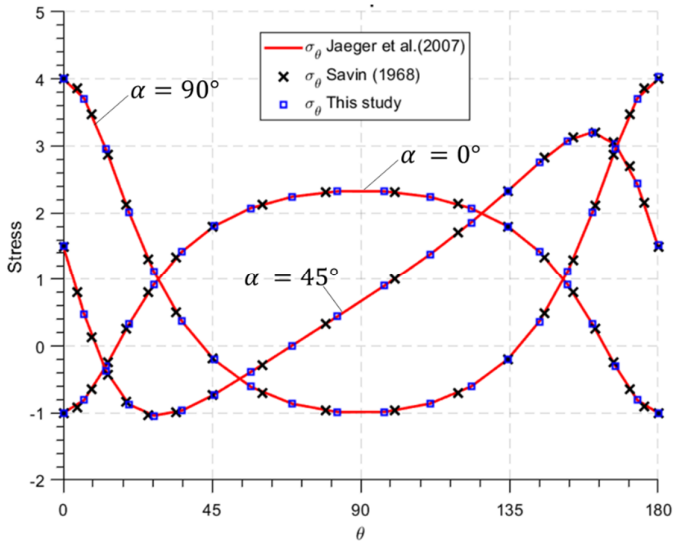

Figure 6. Hoop stress around an elliptical hole having $a/b = 3/2$, in an isotropic medium, subjected to a far-field stress acting at an angle α to the x-axis. The hoop stress is normalised against the far-field stress.

The proposed method can also be tested against results for an elliptical hole in an anisotropic medium. Savin[6] considered an anisotropic material with a Young's modulus ratio of $E_1/E_2 = 12$. For this material, the roots of the characteristic equation are $\mu_1 = 3.08i$ and $\mu_2 = 1.12i$. Elliptical holes with $a/b = 3$ and $a/b = 1/3$ were considered, and the far-field stress was taken to be parallel to the x-axis. The normalized hoop stress is plotted in Fig. 7, with the curves showing the values computed by the present method, and the data points taken from Tables 38 and 39 of Savin[6]. Again, the agreement is excellent.

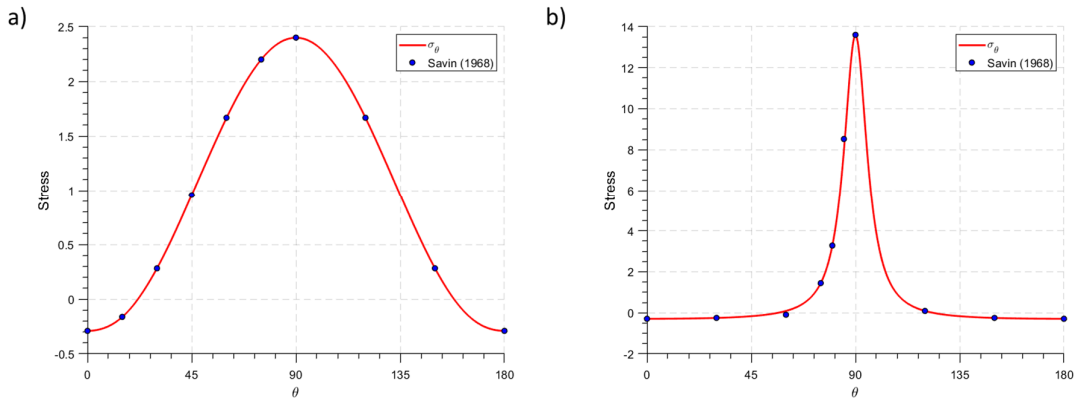

Figure 7. Normalised hoop stress around elliptical holes in an anisotropic medium, having (a) $a/b = 3$ and (b) $a/b = 1/3$, subjected to a far-field stress parallel to the x-axis. The curves show the values computed by the present method; the data points are taken from Savin[6].

5.2 Triangular hole

The distribution of stress around a triangular hole is given by Savin[6] for the case of an isotropic material. The equation of the hole contour was given by

$$x = \cos\theta + \frac{1}{3}\cos 2\theta\,, \quad y = -\sin\theta + \frac{1}{3}\sin 2\theta \tag{69}$$

which corresponds to a triangle that is "pointing towards" the positive x-axis. Using Melentiev's approximate method, the conformal mapping constants of this triangle are found to be $m_0 = 0.9978$, $m_1 = 0.0020$, $m_2 = 0.0019$, $m_3 = 0.3303$, $m_4 = 0.0006$, $m_5 = 0.0002$ and $m_6 = m_7 = m_8 = m_9 = 0.0001$. The stress distributions around the triangular hole, for the two cases in which the far-field stress is parallel to the x-axis or parallel to the y-axis, are shown in Fig. 8. The results of the present method, shown as solid curves, are in an excellent agreement with those of Savin, which are shown as dots taken from Tables 5 and 6 of Savin[6].

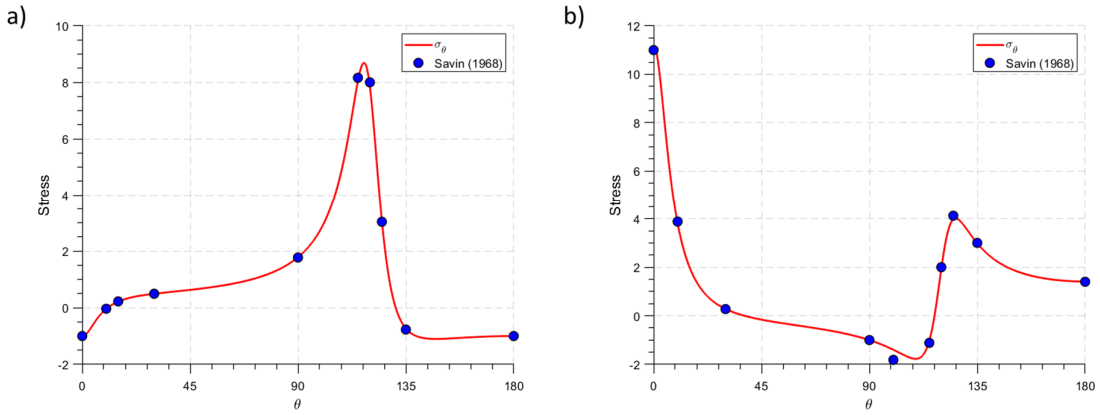

Figure 8. Normalised hoop stress around a triangular hole in an isotropic infinite plates, when the far-field stress is aligned with the (a) x-axis or the (b) y-axis. The solid curves are the predictions of the present method; the dots are taken from Savin[6].

Daoust and Hoa[1] proposed an analytical solution for a family of quasi-triangular holes in isotropic or anisotropic materials. The shape of their triangles was controlled by a shape factor ε, in which smaller values of ε correspond to more rounded corners:

$$x = \cos\theta + \varepsilon\cos 2\theta\,, \qquad y = -\sin\theta + \varepsilon\sin 2\theta \tag{70}$$

The shapes of the triangles for $\varepsilon = 1/4$ and $\varepsilon = 1/8$ are shown in Fig. 9, on the left. The tangential stresses around the contour are plotted for several values of ε, with the curves showing the predictions of the present method, and the data points taken from Daoust and Hoa[1]. Note that the curve for $\varepsilon = 1/3$ agrees closely with Savin's result, which corresponds to this same value of ε. Again, the newly computed values agree very closely with the values taken from the literature.

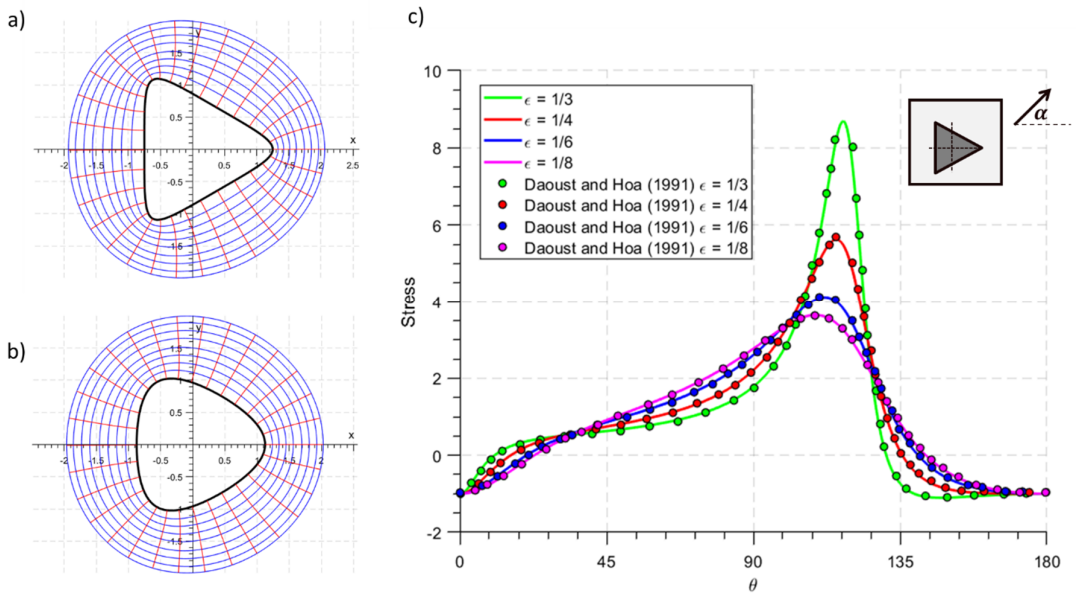

Figure 9. Quasi-triangular holes described by eq. (53), for (a) $\varepsilon = 1/4$ and (b) $\varepsilon = 1/8$. (c) Normalised hoop stress around the hole, in an isotropic material, when the far-field stress is aligned with the x-axis, for various values of ε. The solid curves are the predictions of the present method; the dots are taken from Daoust and Hoa[1].

Daoust and Hoa[1] also considered an anisotropic plate described by the following roots of the characteristic equation: $\mu_1 = 2.3992i$ and $\mu_2 = 0.6757i$. The tangential stress along the hole is shown in Fig. 10, for the case $\varepsilon = 1/3$, and a far-field stress aligned with the x-axis. The agreement is again very good.

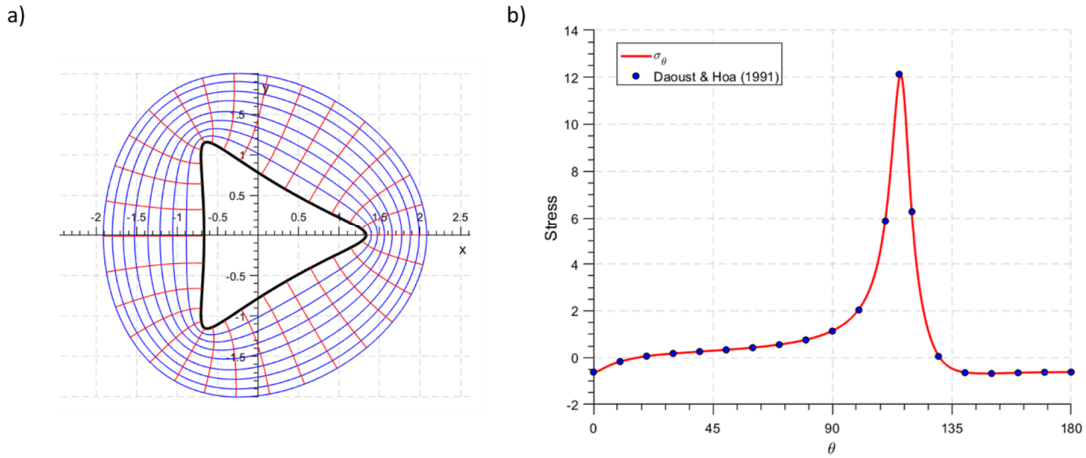

Figure 10. Quasi-triangular hole described by eq. (70), for $\varepsilon = 1/3$, in an anisotropic material (see text for details), when the far-field stress is aligned with the x-axis. The solid curves are the values obtained by the present method; the dots are taken from Daoust and Hoa[1].

5.3 Ovaloid hole

Greenspan[4] presented an analytical solution for an "ovaloid" hole in an infinite isotropic plate subjected to far-field uniaxial tension. He defined the ovaloid as a square hole with semi-circles appended at each of two opposing ends, and described its contour by the following equation:

$$x = 2.063\cos\theta - 0.079\cos 3\theta\,, \quad y = 1.108\sin\theta + 0.079\sin 3\theta \tag{71}$$

(Lekhnitskii[5] also addressed this problem, but used a slightly different equation for the hole that he described as "ovaloid", which explains the slightly different stresses obtained by these two authors). Greenspan showed that when the far-field stress is parallel to the x-axis, the hoop stress is given by

$$\sigma_\theta = \sigma_x^\infty \left[\frac{4.915 - 7.133\cos 2\theta}{3.723 - 2.316\cos 2\theta + \cos 4\theta}\right] \tag{72}$$

and when the far-field stress is parallel to the y-axis, the hoop stress is given by

$$\sigma_\theta = \sigma_y^\infty \left[\frac{1.079 + 7.517\cos 2\theta}{3.723 - 2.316\cos 2\theta + \cos 4\theta}\right] \tag{73}$$

In the present study, the conformal mapping constants of the ovaloid defined in eq. (71) are found to be $m_0 = 1.5818$, $m_1 = 0.0029$, $m_2 = 0.4768$, $m_3 = -0.0003$, $m_4 = -0.0771$ and $m_5 = -0.0003$. The hoop stresses for the two loading cases, according to the analytic solution of Greenspan[4] and the present method, are shown in Fig. 11. Again, the agreement is very good.

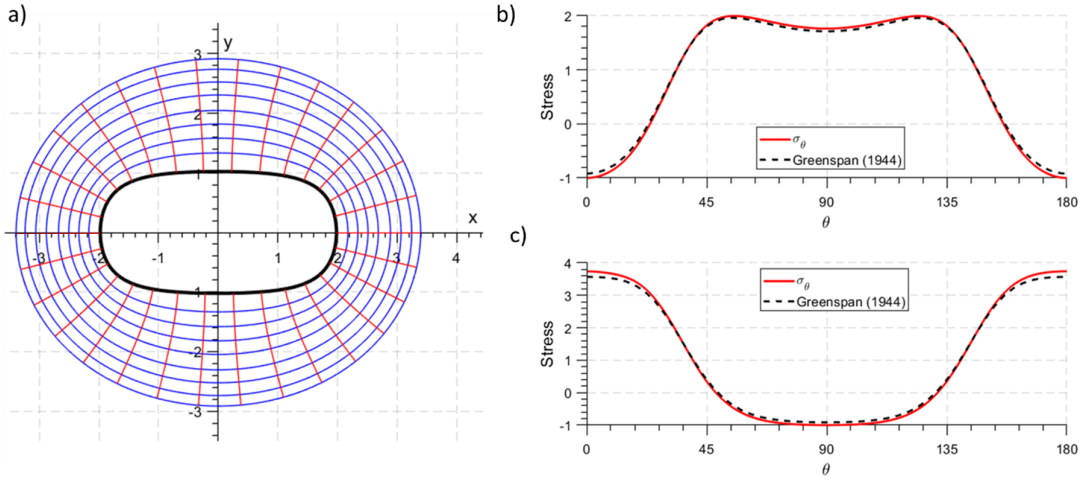

Figure 11. (a) Ovaloid hole described by eq. (71). Normalised hoop stresses when the far-field stress aligned with the x-axis (b), and with the y-axis (c). Solid curves are the predictions of the present method, and dashed curves are expressions (72) and (73) derived by Greenspan[4].

5.4 Square hole

Stresses around a square hole in an infinite plate subjected to a far-field stress have been studied by many authors, including Greenspan[4], Lekhnitskii[5], and Savin[6]. Savin modelled a square hole using two terms of the Schwarz-Christoffel mapping:

$$x = \cos\theta - \frac{1}{6}\cos 3\theta, \quad y = -\sin\theta - \frac{1}{6}\sin 3\theta \tag{74}$$

and showed that the tangential stress around this hole is given by

$$\sigma_\theta = \frac{8\sigma^\infty}{5 + 4\cos 4\theta}\left(\frac{3}{8} - \frac{9}{7}\cos 2\alpha \cos 2\theta - \frac{3}{5}\sin 2\alpha \sin 2\theta\right) \tag{75}$$

where again α denotes the angle of rotation from the x-axis to the line of action of the far-field stress.

Using Melentiev's method, the conformal mapping constants of this quasi-square defined by eq. (74) are found to be $m_0 = 0.9975$, $m_1 = 0.0012$, $m_2 = 0$, $m_3 = -0.0011$, $m_4 = -0.1629$, $m_5 = -0.0009$, $m_6 = -0.0002$ and $m_7 = -0.0001$. The hoop stresses for the two loading cases of $\alpha = 0°$ and $\alpha = 45°$, are shown in Fig. 12, according to the analytic solution of Savin[6] and the present method.

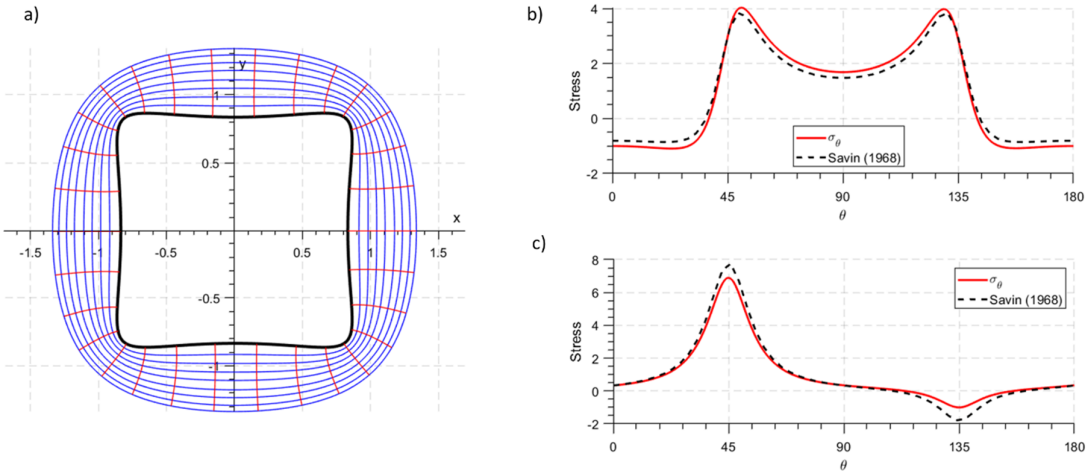

Figure 12. Stress around a quasi-square hole (a) in isotropic medium, when the external load is (b) aligned with the x-axis, and (c) rotated by 45° from the x-axis. The solid curves are the predictions of the present method, and the dashed curves are from the analytical solution derived by Savin[6].

Ukadgaonker and Rao[20] considered terms up to ξ^{-19} in their conformal mapping, in order to obtain a closer approximation to an actual square. The non-zero coefficients in their

mapping function were (in the present notation) $m_0 = 1$, $m_4 = 1/6$, $m_8 = 1/56$, $m_{12} = 1/176$, $m_{16} = 1/384$ and $m_{20} = 7/4864$. They considered an anisotropic material whose characteristic roots were $\mu_1 = 3.6404i$ and $\mu_2 = 0.2747i$. For the cases of far-field loading oriented at angles of $\alpha = 0°$, 45°, and 60°, the hoop stresses are shown in Fig. 13, where they are compared with the values obtained by the present method. The agreement is very good, and the present method is clearly able to capture the high stress concentration at the corners.

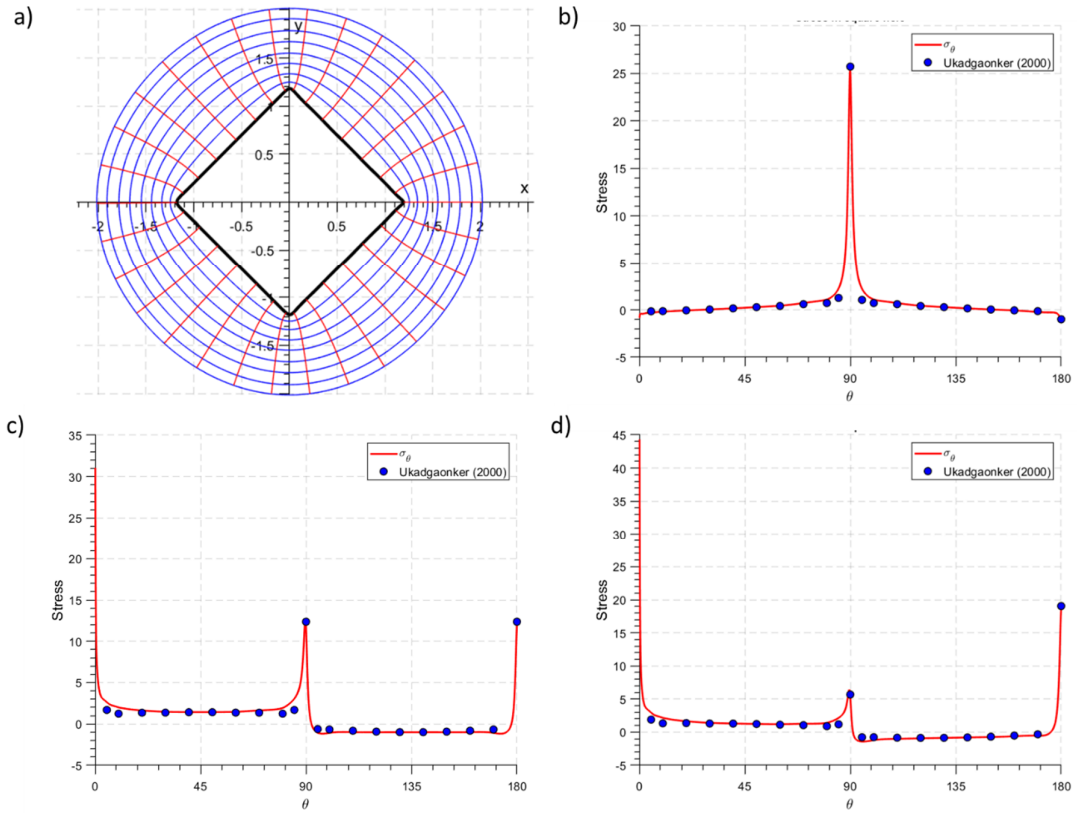

Figure 13. Hoop stress around a square hole, for far-field loadings at angles of $\alpha = 0°$, 45°, and 60°, in an anisotropic medium whose characteristic roots are $\mu_1 = 3.6404i$ and $\mu_2 = 0.2747i$. The solid curves are the predictions of the present method, and the points are from Ukadgaonker and Rao[20].

Ukadgaonker and Rao[20] also considered more complicated shapes, such as the distorted quasi-square with truncated corners shown in Fig. 14. For the same anisotropic material as considered in the previous problem, with characteristic roots of $\mu_1 = 3.6404i$ and $\mu_2 = 0.2747i$, the hoop stresses are shown in Fig. 14, for the case of loading along the x-axis, *i.e.*, $\alpha = 0°$. The agreement between their results and those obtained by the present method is

reasonably close.

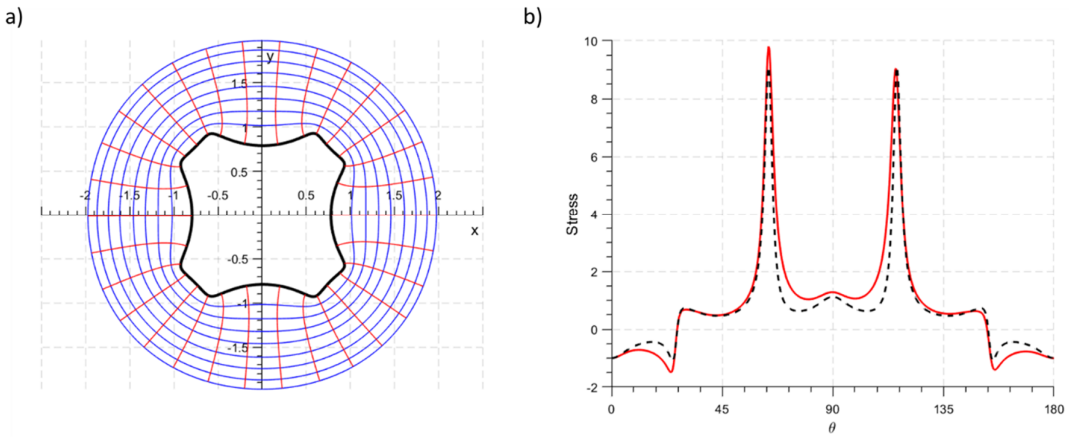

Figure 14. (a) A distorted quasi-square with truncated corners. (b) Normalised hoop stress around the hole, for a far-field loading oriented in the x-direction, in an anisotropic medium whose characteristic roots are $\mu_1 = 3.6404i$ and $\mu_2 = 0.2747i$. Solid curves are the predictions of the present method; dashed curves are from Ukadgaonker and Rao[20].

6. Stress around a non-symmetrical and irregularly shaped hole

The previous examples all involved holes having some degree of symmetry, and shapes that were in some sense reasonably "simple", such quasi-polygons. However, this unified methodology that can compute the stresses around an arbitrarily-shaped hole will perhaps find its greatest usefulness for holes that have very irregularly and rough shapes.

One source of such shapes are subsurface boreholes, which are initially drilled as circular holes, but then often suffer from "breakouts", in which small regions of rock at the borehole wall break off (and fall into the borehole, to be swept away by the drilling fluid) due to local failure, leading to a non-circular shape. The remaining rock can be treated as elastic, and the method developed in this paper can be used to compute the new stresses, to check if an equilibrium shape has been reached. Pre-drilling wellbore stability analysis is often carried out by assuming a circular wellbore and with the aid of a downhole caliper tool, and it is known that actual wellbores rarely have the shape of an ideal circle. It is of great interest for drilling practice to understand the stability of a wellbore by identifying the region around the wellbore wall that has a high stress concentration.

Although extensive examples will be the subject of a future paper, one example will be given here to illustrate the potential usefulness of the new methodology. Zoback *et al.*[19] presented several wellbore shapes reconstructed from ultrasonic borehole televiewer images. In the present paper, one of the wellbore shapes reported by Zoback *et al.*[19] has been

digitized, and the stress around the wellbore wall has been calculated, using the methodology outlined above. The tangential stresses shown in Fig. 15 indicate the compressive and tensional regions around the wellbore. As expected, high stress concentrations occur around the wellbore at locations that have relatively sharp edges.

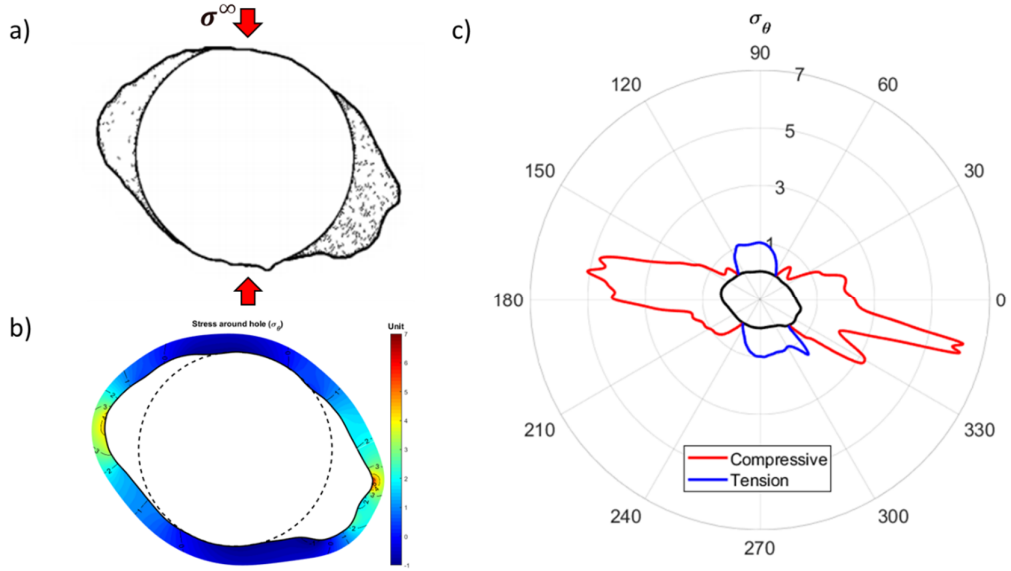

Figure 15. (a) Wellbore breakout in and isotropic medium, after Zoback *et al.*[19], and (b,c) the tangential stress around the hole, under uniaxial far-field compression.

7. Validity of Solution away from the Hole Contour

Although the method used to determine the mapping functions was different, the method used in the present paper to determine the complex potentials is very close to that used by Ukadgaonker and Rao[20]. Their method was criticised by Lu *et al.*[12], who claimed that the potentials $\phi_0(\xi)$ and $\psi_0(\xi)$ thus derived will be analytical functions on the hole contour, but will *not* be analytical in the region exterior to the contour; see [12] for the details of their argument. They concluded that although the computed stresses will be correct on the hole boundary, the stresses away from the boundary "should not be correct", although no evidence was given of this assertion.

To verify the validity of the stresses computed by the present methodology at points in the body that are not situated along the hole contour, comparison can be made to the stresses that were computed numerically by Lu *et al.*[12], using commercial finite element software, around a "Reuleaux triangle" hole in an orthotropic material; see Figs. 10-12 in [12], and Fig. 16 below. This is one of the few, if not the only, examples available in the literature in which

the stresses have been plotted along one of the co-ordinate axes, moving away from a non-circular hole in an anisotropic material. In this example, the elastic anisotropy was characterised by $\mu_1 = 1.3733i$ and $\mu_2 = 0.9242i$, and the far-field stress state was taken to be $\sigma_{xx}^{\infty} = 10$ MPa, $\sigma_{yy}^{\infty} = 15$ MPa, and $\sigma_{xy}^{\infty} = 0$ MPa.

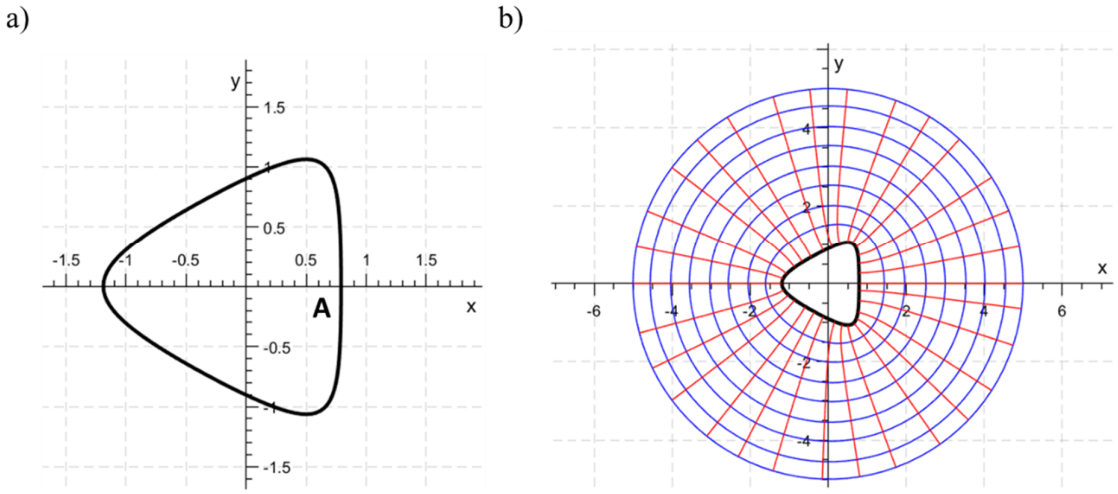

Figure 16. (a) The Reuleaux triangle shape, and (b) the conformal mapping of the hole.

The hoop stresses along the hole boundary that have been computed using the proposed method are compared in Fig. 17b against those computed numerically in [12]. The agreement is excellent. The stress components σ_{xx} and σ_{yy}, along the x-axis, are plotted in Fig. 17b. Again, the agreement between the present method and the numerical calculations of [12] is excellent. Furthermore, it should be noted that the stresses computed by the present methodology converge smoothly to the correct far-field stresses at distances of roughly five "hole diameters" from the hole boundary, proving that the present methodology does not become inaccurate away from the hole.

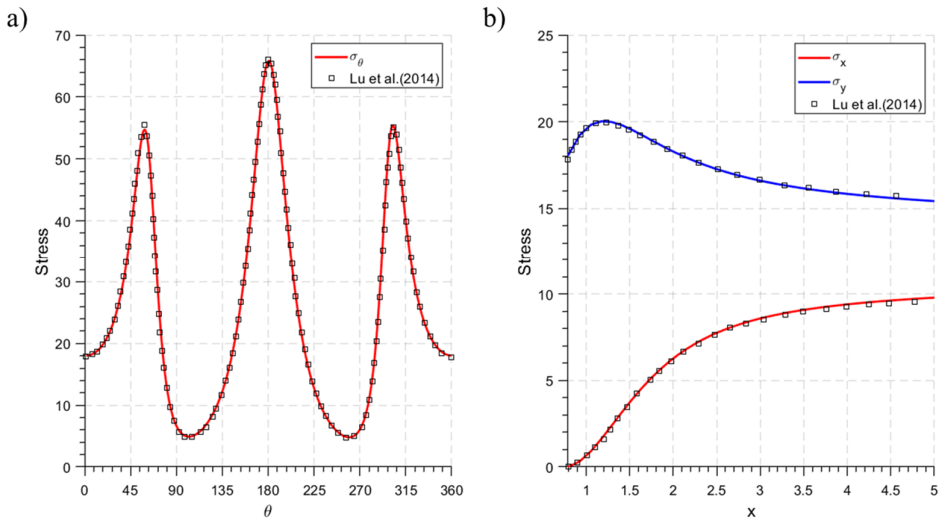

Figure 17. (a) The hoop stresses around the Reuleaux triangular hole boundary shown in Fig. 16, and (b) the two normal stresses along the x-axis. The symbols are the values computed in [12] using finite elements; the curves show the stresses computed by the present method.

8. Conclusions and Discussion

A unified method has been presented in which the stress distribution around an arbitrary cross-sectional hole is calculated by coupling the graphical conformal mapping of Melentiev, with the complex stress potential method. A new representation of the stress potentials has been derived which depends on the conformal mapping constants obtained using Melentiev's iterative procedure. The method allows the calculation of the in-plane stress components around an arbitrary hole for any given contour shape, in isotropic or anisotropic media. Validation against several known results has been carried out for a wide range of hole shapes and anisotropic materials, including non-symmetrical and irregular shape such as wellbore breakouts. The methodology has also been shown to yield accurate stresses in the "interior" of the material, away from the hole boundary. The method therefore provides a unified and accurate approach for studying the effect of hole geometry on stress distribution around holes in isotropic or anisotropic materials, and should be particularly useful for irregularly-shaped holes that are not symmetrical or quasi-polygonal.

Acknowledgements

This study was supported by the Indonesian Endowment Fund for Education (LPDP) of the Republic of Indonesia. The authors thank the anonymous reviewers for their very thoughtful and insightful comments, which have greatly helped us to improve the rigor and clarity of the paper.

References

1. Daoust, J. and S. Hoa, An analytical solution for anisotropic plates containing triangular holes. Composite Structures, 1991. 19(2): 107-130.

2. Gercek, H. Stresses around tunnels with arched roof. In: Proc. 7th ISRM Congress. 1991. International Society for Rock Mechanics.

3. Gercek, H. An elastic solution for stresses around tunnels with conventional shapes. International Journal of Rock Mechanics and Mining Sciences, 1997. 34(3): 96.e1-96.e14.

4. Greenspan, M. Effect of a small hole on the stresses in a uniformly loaded plate. Quarterly of Applied Mathematics, 1944. 2(1): 60-71.

5. Lekhnitskii, S. G., Anisotropic Plates. 1968, Gordon and Breach, New York.

6. Savin, G. N., Stress Concentration around Holes. 1961, Pergamon Press, Oxford.

7. Kolosov, G. V., On the Application of the Theory of Functions of a Complex Variable to a Plane Problem in the Mathematical Theory of Elasticity, PhD. Diss., Dorpat University (in Russian), 1909.

8. Muskhelishvili, N. I., Some Basic Problems of the Mathematical Theory of Elasticity. 1953, Nordhoff, Groningen.

9. Driscoll, T. A. and L. N. Trefethen, Schwarz-Christoffel Mapping. 2002, Cambridge University Press, Cambridge.

10. Melentiev, P. V., Several New Methods and Devices for Approximate Computations. 1937, Moscow-Leningrad.

11. Simha, K. R. Y. and S. S. Mohapatra, Stress concentration around irregular holes using complex variable method. Sadhana, 1998. 23(4): 393-412.

12. Lu, A. Z., N. Zhang, X. L. Zhang, and D. H. Lu, Analytic method of stress analysis for an orthotropic rock mass with an arbitrary-shaped tunnel. International Journal of Geomechanics, 2015. 15(4): 04014068.

13. Mitchell, L. H., Stress-concentration factors at a doubly-symmetric hole. Aeronautical Quarterly, 1965. 17(2): 177-186.

14. Exadaktylos, G. E., P. A. Liolios, and M. C. Stavropoulou, A semi-analytical elastic stress–displacement solution for notched circular openings in rocks. International Journal of Solids and Structures, 2003. 40(5): 1165-1187.

15. Exadaktylos, G. E. and M. C. Stavropoulou, A closed-form elastic solution for stresses and displacements around tunnels. International Journal of Rock Mechanics and Mining Sciences, 2002. 39(7): 905-916.

16. Sobey, A. J., The estimation of stresses around unreinforced holes in infinite elastic sheets. Aeronautical Research Council Reports and Memoranda, Ministry of Aviation, HM Stationery Office, 1964.

17. Kantorovich, L. and V. Krylov, Approximate Methods of Higher Analysis, 1958, Noordhoff, Groningen.

18. Gaede, O., F. Karpfinger, J. Jocker, and R. Prioul, Comparison between analytical and 3D finite element solutions for borehole stresses in anisotropic elastic rock. International Journal of Rock Mechanics and Mining Sciences, 2012. 51: 53-63.

19. Zoback, M. D., D. Moos, and L. Mastin, Wellbore breakouts and in situ stress. Journal of Geophysical Research, 1985. 90(B7): 5523.

20. Ukadgaonker, V. G. and D. K. N. Rao, A general solution for stresses around holes in symmetric laminates under inplane loading. Composite Structures, 2000. 49(3): 339-354.

21. Lekhnitskii, S. G., Theory of Elasticity of an Anisotropic Elastic Body. 1963, Holden-Day, San Francisco.

22. England, A. H., Complex Variable Methods in Elasticity. 2003, Dover, Mineola, NY.

23. Jaeger, J. C., N. G. W. Cook, and R. W. Zimmerman, Fundamentals of Rock Mechanics, 4th ed. 2007, Wiley-Blackwell, Oxford.